Capillary drainage of a sessile droplet through a hole

Songlin Shi [1,2] Jinlong Song,[3] Bin Zhang [1] Chen Ma,[1,2] Pan Jia,[4] and Cunjing Lv [1,2,*]

[1]*Department of Engineering Mechanics, Tsinghua University, 100084 Beijing, China*

[2]*Center for Nano and Micro Mechanics, Tsinghua University, 100084 Beijing, China*

[3]*Key Laboratory for Precision and Non-Traditional Machining Technology of Ministry of Education, Dalian University of Technology, 116024 Dalian, China*

[4]*School of Science, Harbin Institute of Technology, 518055 Shenzhen, China*

(Received 2 June 2020; accepted 24 August 2020; published 2 October 2020)

In this paper, we investigate drainage and oscillation behaviors of sessile drops caused by capillary drainage through a hole. When a water drop is deposited on a hole drilled on a superhydrophobic plate in contact with a bath of water from the bottom side, the liquid in the drop will transport into the bath and a jet is then produced. We focus on the evolution of the drop diameter $D(t)$ with time t. For a small drop, a scaling relation $D(t) \sim t^{2/7}$ is observed, arising from the competition between the surface tension and inertia. In addition, due to the initial perturbation arising from the deposition, both the drop and the jet show oscillation behaviors. It is observed that the amplitude of the drop oscillation decreases with time while the frequency increases, and we attribute these behaviors to the variable drop mass as well as the competition between the capillary force and the inertia. Considering the present system as a damped harmonic oscillator with variable mass, theoretical models are proposed, which predict well the experimental results. Moreover, we develop a way to suppress the initial perturbation, which allows us to create drops with very large volumes. Our results show that the scaling regime asymptotically reaches $D(t) \sim t^{1/2}$ when the drop becomes a puddle.

DOI: 10.1103/PhysRevFluids.5.104002

I. INTRODUCTION

Capillary-driven flows are ubiquitous in nature and industry. Investigating flows driven by capillary forces through a hole is of fundamental importance to understand a variety of natural and industrial processes, such as drinking strategies of animals [1,2], oil extraction [3,4], flows in porous media such as soil science and powder technology [5–8], suspensions and emulsion stability [9,10], pumps in plants [11,12], and energy applications [13], and micro- and nanofluidics [14,15].

One of the most classic phenomena of the capillary flows is the capillary rise [16]. When one end of a capillary tube is put in contact with water, due to the capillary force, a meniscus liquid-air interface appears in the tube and climbs along the inner wall of the capillary. This well-known phenomenon results from a balance between surface tension and viscous resistance. As a consequence, the length of the liquid column increases as the square root of time, generally referred as the Lucas-Washburn law [17,18]. So far, researchers have developed more complete models to describe the dynamics of the process. It showed that for inviscid liquid, the dynamic behavior deviates from the Lucas-Washburn law at short time, due to inertia [6,19,20]; and moreover, deviations were observed at long time due to gravity [18,21]. In addition, the contact line pinning is often unavoidable for a real system, Lavi *et al.* [6] and Hamraoui *et al.* [22] showed that other deviations

*cunjinglv@tsinghua.edu.cn

arise from the additional dissipation associated with the motion of a contact line at the top of the moving liquid-vapor meniscus. In contrast with the traditional view, Delannoy *et al.* studied the reverse capillary rise phenomenon, in which capillary descent with a linear velocity were observed when a superhydrophobic capillary tube was immersed in water [23].

Beyond the transport stage, researchers have spent a lot of attention on the oscillation behaviors close to the balance point. When a liquid of very low viscosity is contained in the capillary tube and the Jurin's height [16] is reached, it has been found that oscillations occur due to inertia. In this case, the liquid-vapor meniscus is damped and the oscillation is nonlinear (parabolic) because of the nonconstant mass of the oscillator [19]. Considering the dissipations resulting from the irreversible energy loss at the entrance of the tube and the viscous friction inside it, the threshold in viscosity above which oscillations disappear was calculated [19]. For the inverted capillary rise phenomena [23], the combination of the viscous friction, gravity force and inertia of water could also lead to oscillation behaviors, and the threshold for the oscillation was quantified by the tube length and radius. Moreover, experimental investigations on capillary rise phenomena in closed capillary tubes were also reported [24,25], but the oscillatory behavior of the meniscus was not observed due to the friction of the moving contact line.

Despite the fact that the capillary-driven flows have been studied for a long time, there has been a renewed interest in it because of its great importance in biological function, microfluidic devices and materials processing. In recent years, researchers developed various physicochemical methods to extend this phenomenon to much broader regimes. In very small scale, spontaneous absorption driven by surface tension was studied in the context of metallic liquid droplets and carbon nanotubes [26], because of carbon nanotubes filled with metal nanoparticles showing promising applications in treatment of cancerous tumors [27,28]. By employing sessile drops and containers with holes, power-free pumps having the functions such as spontaneous anti-gravity and long-distance water delivery were realized thanks to the capillary force [29–31]. Because of the surface tension, small bubbles always empty into the larger ones, which triggers the foam coarsening and instability, and determines the foam's useful lifetime [9]. Moreover, researchers employed the pressure difference between small and large droplets to transport water to enhance dropwise condensation and water harvesting [32].

Even though achievements are obtained, we report in this work, among others, drainage and oscillation behaviors of drops driven by capillary forces through a hole. In our case, when a drop is deposited on a hole drilled on a superhydrophobic plate in contact with a bath of water from the bottom side, Laplace pressure will drive a flow that transports water from the drop to the bath and meanwhile creates a jet in the bath. Despite all the efforts described aforementioned, the underlying mechanism of this phenomenon has still been largely unexplored. To close the gap, we investigate the drainage and the oscillation behaviors of drops driven by the capillary flow over a broad range of parameters, such as the hole diameter and the size of the drops. We hope our results will enhance the understanding of capillary phenomena and find practical applications in water harvesting and filtering.

The paper is organized as following. In Sec. II, experimental procedures are described. In Sec. III, theoretical models are proposed to explain the evolution of the drop, as well as the associated oscillation behaviors. In Sec. IV, we carry out experiments by employing a way to suppress the oscillation, and we focus on the two scaling regimes. Final concluding remarks are given in Sec. V.

II. EXPERIMENTS

A. Experimental setup

The experiment setup consists of a needle, a pump, a superhydrophobic aluminum (Al) plate with a hole, and a container filled with water [Fig. 1(a)]. The horizontal section of the container is 7.4×4 cm, and its depth is 15 cm. The Al plate is machined into square shape with a width of 4 cm and a thickness of 400 μm. To make the Al plate superhydrophobic, we follow a method reported in

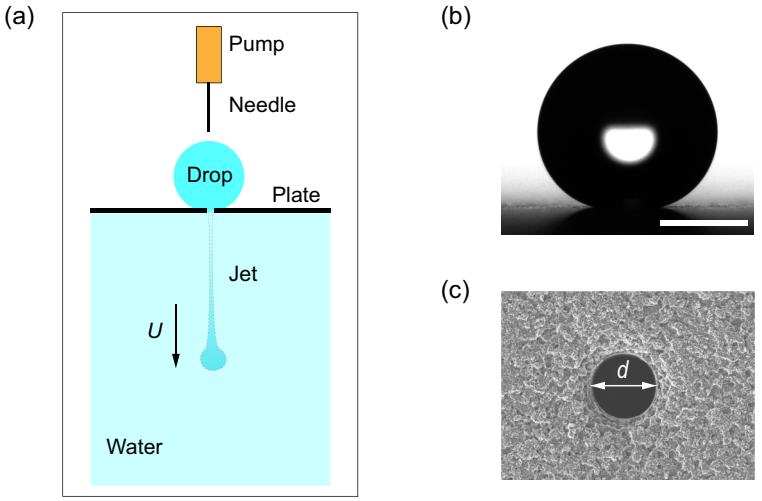

FIG. 1. Experimental setup and samples. (a) Schematic of the experimental setup, which consists of a needle, a pump, a superhydrophobic Al plate with a hole in the center, and a container filled with water. (b) Wetting state of a 3.9 μl sessile drop on the superhydrophobic Al plate. The contact angle is $\theta^* = 158 \pm 2^\circ$. The scale bar represents 1 mm. (c) Scan Electronic Microscope (SEM, JSM-IT300) imaging of the superhydrophobic Al plate with a hole. The diameter of the hole is $d = 200$ μm.

Huang *et al.* [30], which leads to an apparent contact angle $\theta^* \approx 158 \pm 2^\circ$ [Fig. 1(b)]. After that, we drill a hole in the center of the plate via a precision bench drill [Fig. 1(c)], which leaves a hydrophilic inner wall since aluminum is exposed. Seven samples are prepared with hole diameters d ranging from 100 to 700 μm.

In our experiments, we first fill the container with water, and then put the Al plate on the top of water. Water is absorbed immediately into the hole because of the hydrophilic nature of the inner wall of the hole. For a better visualization, water is dyed in advance using blue ink at a very low concentration (ink/water <5% (v/v)), so the variation of the water surface tension σ is negligible. By employing a pump and a needle with different diameters, we are able to quasistatically create drops with various volumes Ω_0. By an electronic balance, we first measure the total mass of 100 continuous drops, and then we calculate Ω_0 based on the average value and the mass density of water. The needle is placed on top of the hole. When the drop becomes big enough, it naturally detaches from the needle tip. To suppress additional inertial force brought by the falling drop, we try our best to shorten the distance between the hole and the bottom of the drop at the moment when the drop is dripping.

B. Observations

As shown in Fig. 2(a) with a hole diameter of 200 μm, from the moment that the drop ($\Omega_0 = 5.8$ μl) attaches the Al plate, its content is pushed into the lower bath through the hole (see movie 1 in the Supplemental Material [33]). We also observe oscillations of the drop during the drainage (more details will be given in the next section), but in this case the oscillation is weak in the image sequences of Fig. 2. Meanwhile, as shown in Fig. 2(b), a starting jet with a toroidal (mushroomlike) vortex at its front is generated in the bath ($\Omega_0 = 3.8$ μl, see movie 2 in the Supplemental Material [33]). For a better visualization, we demonstrate these processes in Fig. 2(a) and Fig. 2(b) separately. Even though the drop has totally disappeared (i.e., at 144.4 ms), the jet continues to move forward and lasts a while.

Next, we check the influence of the hole diameter on the drainage dynamics of the drop. As shown in Fig. 3 with a hole diameter of 600 μm, we observe similar dynamic phenomena as shown in

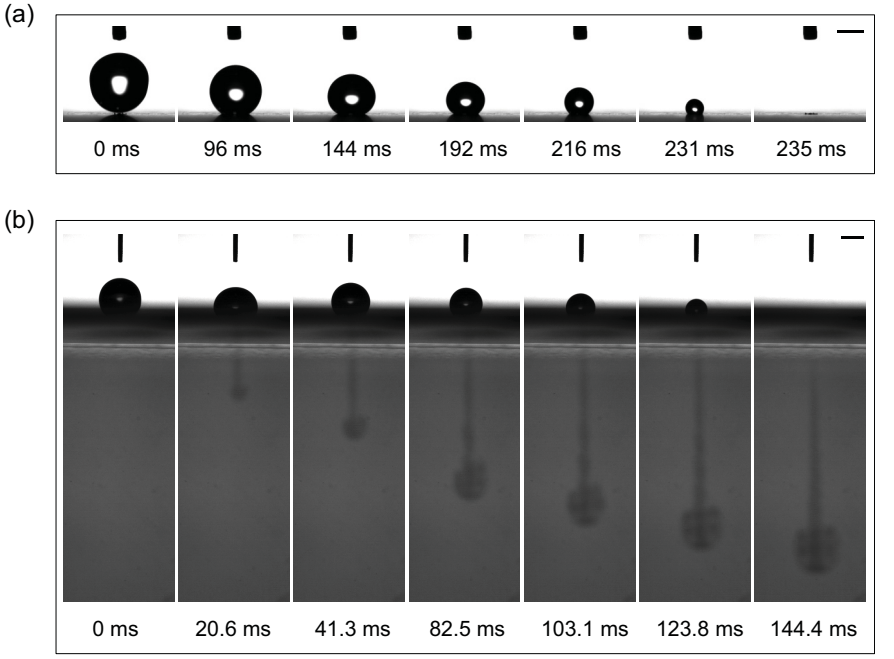

FIG. 2. Evolution of the drop and the jet. The diameter of the hole is 200 μm. (a) Details of the drainage of the drop. The video is recorded at 4000 fps. The initial volume of the drop is 5.8 μl. (b) The evolution of the jet. The video is recorded at 3200 fps. The initial volume of the drop is 3.8 μl. The scale bars represent 1 mm.

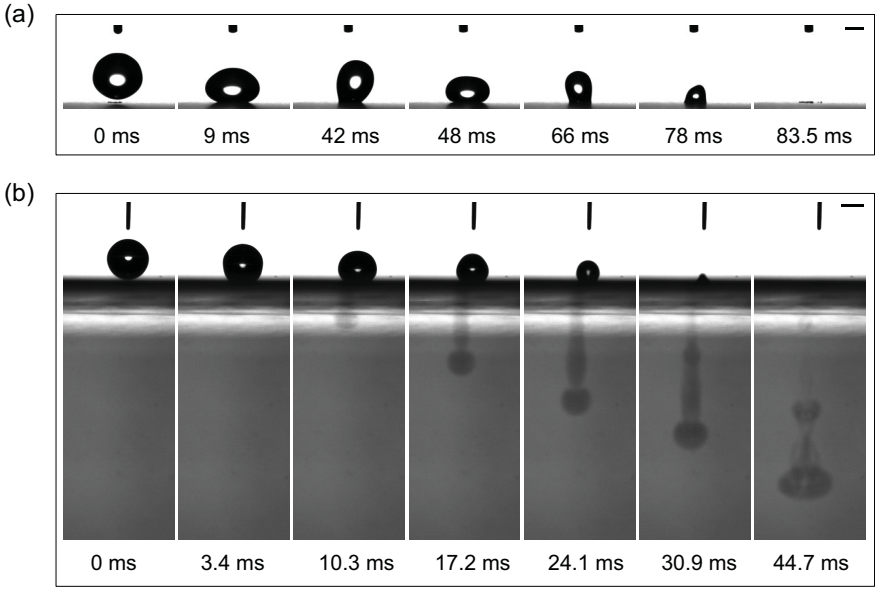

FIG. 3. Evolution of the drop and the jet. The diameter of the hole is 600 μm. (a) Details of the drainage of the drop. The video is recorded at 4000 fps. The initial volume of the drop is 9.5 μl. (b) The evolution of the jet. The video is recorded at 3200 fps. The initial volume of the drop is 3.8 μl. The scale bars represent 1 mm.

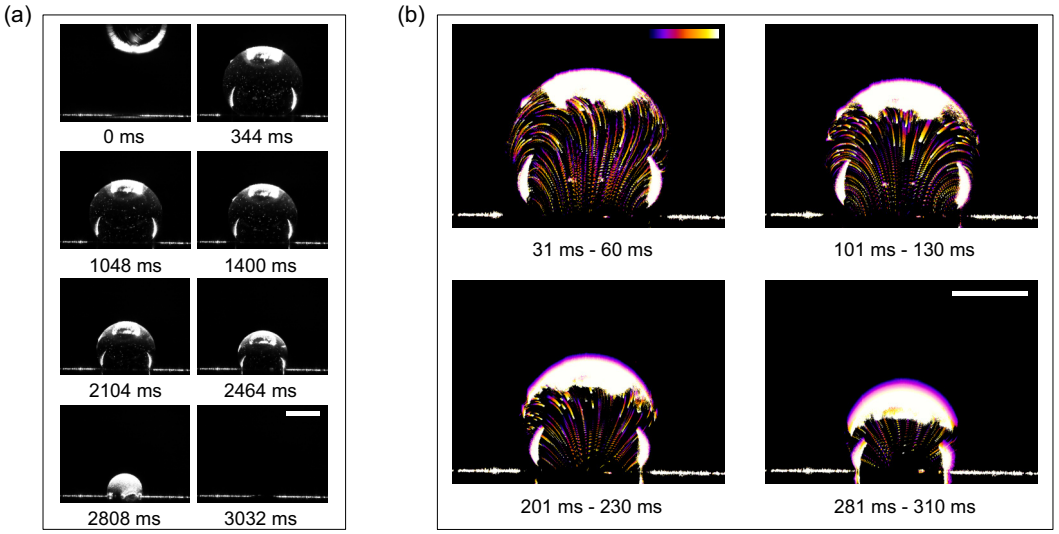

FIG. 4. Inner flow fields of the drop captured by micro-PIV. (a) Inner flow with fluorescent particles under a laser sheet. (b) Color time-lapse images during different stages. The color scale bar shows the frame varying with time. The volume of the drop is 5.8 μl, corresponding to an initial diameter of 2.3 mm. The scale bars represent 1 mm.

Fig. 2. However, Fig. 3(a) shows more obvious oscillations of the drop during the drainage process (see movies 3 and 4 in the Supplemental Material [33]), which is remarkably different from the typical oscillation of a sessile drop with a fixed volume [34–36]. Moreover, for drops with the same volume (i.e., $\Omega_0 = 3.8$ μl), the depletion time of the drop [∼40 ms, see Fig. 3(b)] is much smaller than the smaller hole [∼140 ms, see Fig. 2(b)]. Here, the depletion time is defined as the duration from the moment when the drop touches the hole to the moment that it totally disappears.

C. Inner flow fields

To understand the underlying mechanisms, as shown in Fig. 4(a), we carry out experiments via a micro resolution particle image velocimetry (micro-PIV) to capture the inner flow field of the drop. Fluorescent particles with a diameter of 1 μm are first added into the drops. The fluorescent particles are polystyrene microspheres, and the mass density is 1.055 g/mm^3 (Invitrogen Corporation, F13082). A laser sheet from a semiconductor laser (1500 mW, 532 nm) is created and focuses on the meridian plane of the drop. For a better visualization, the images of the drop and the jet are acquired separately. Because of the oscillation of the fluid caused by the initial perturbation, we can only obtain a vivid fluorescence observation of the drop with a hole diameter of 100 μm. When the hole diameter $d \geqslant 100$ μm, the fluorescence observation is pretty scattered.

In Fig. 4(b), we present color time-lapse images of the phenomenon. Each image is a superposition of 30 time-lapse sequences, and the duration is 30 ms. In this way, we are able to visualize the inner flow field of the drop at different stages (see movie 5 in the Supplemental Material [33]). Because of the unavoidable perturbation when the drop touches the Al plate, the left and right sides of the stream lines are not very symmetric at the initial moment. However, after a while (∼100 ms), the inner flow field is quite smooth and symmetric.

Furthermore, we also capture the vivid fluorescence observation of the jet. Generally, we observe three kinds of behaviors of the jets, that we attribute to different initial perturbations. As show in Fig. 5(a) (see movie 6 in the Supplemental Material [33]), in the absence of any visible perturbation, the front of the jet moves forward very steadily, and the axis of the jet is close to a straight

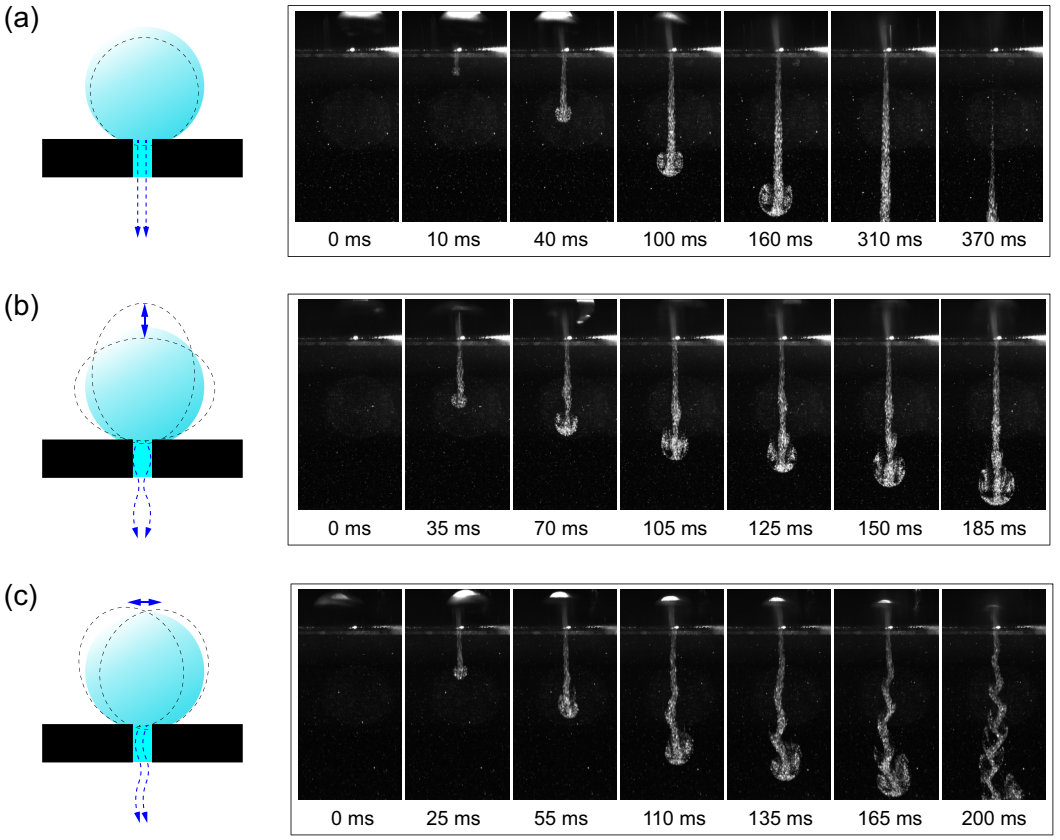

FIG. 5. Three kinds of performance of the jets observed by employing the micro-PIV technique. The left panels are sketches. (a) A steady motion of the jet when the oscillation is very small. (b) A plunging jet. (c) A jet with its trace deviating from its axis. The diameter of the hole is 200 μm. The volumes of the drops are 5.8 μl, corresponding to initial diameters of 2.3 mm.

line. However, if the perturbation is more visible during the deposition of the drop, then the jet demonstrates very different dynamics. As shown in Fig. 5(b) (see movie 8 in the Supplemental Material [33]), if the drop oscillates vertically, then we observe a plunging jet moving forward along its axis. Furthermore, as shown in Fig. 5(c) (see movie 7 in the Supplemental Material [33]), if there are some lateral perturbations, then we observe that the trace of the jet deviates away alternatively from its axis, and it seems that the jet undergoes periodic oscillations by constantly interchanging its position with respect to its axis. Studying/explaining these complex flow phenomena (such as the jet penetration depth, jet liquid column instability, and the deformation of the jet head) in their entirety is a challenging and extensive work going beyond the scope of this paper. Instead, here our attention will be focused on the drainage and the oscillation behaviors of the drop.

III. RESULTS

A. Drainage of the drop

In this section, we describe the underlying mechanisms which controls the drainage behavior of the drop. Experiments are carried out from different views. We first fix the diameter of the hole but vary the initial volume of the drop.

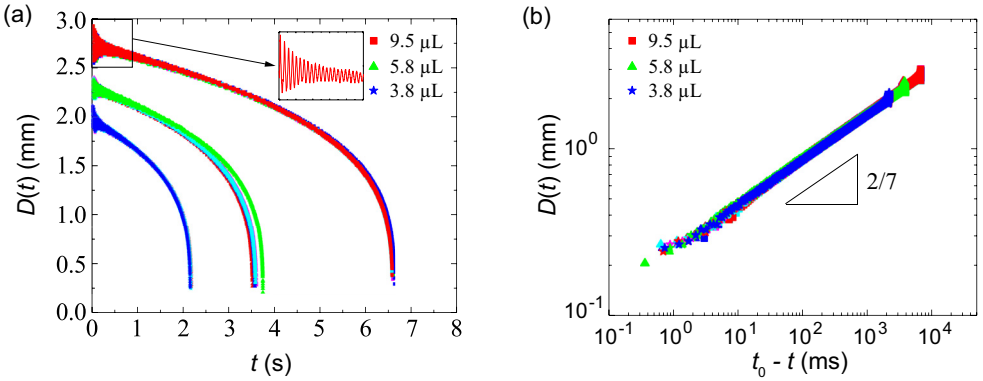

FIG. 6. Evolution of the drop diameter with time. The diameter of the hole is 100 μm. Drops with volumes of 3.8, 5.8, and 9.5 μl are employed, and five tests are carried out for each volume. (a) Evolutions in the normal plot. The inset is an enlargement of the oscillation of the early time. (b) Log-log plot of (a), showing a scaling relation $D(t) \sim (t_0 - t)^{2/7}$.

As shown in Fig. 6 with a hole diameter of 100 μm, the evolutions of the drop diameters (corresponding to initial volumes of 3.8, 5.8, and 9.5 μl) with time are plotted in the linear and log-log plots, respectively. Here, $D(t)$ is defined as the instantaneous lateral diameter of the drop, and t represents the elapsed time starting from the moment that the drop touches the hole. For each volume, five tests are carried out, and we can see there is a very good repeatability and the five curves well overlap each other. For the sake of simplicity, we mark the data of different volumes using the top color of each five tests. In Fig. 6(a), we can see there is an initial slope $dD(t)/dt$ for each volume and the initial slope is smaller when the initial drop volume is bigger. When plotting the experimental data in the log-log diagram, as shown in Fig. 6(b), a scaling relation $D(t) \sim (t_0 - t)^{2/7}$ is observed. Here, we define t_0 as the depletion time, in other words, $D(t = t_0) = 0$.

To deepen our understanding, as shown in Fig. 7, we monitor the evolution of the drop diameter by using hole diameters ranging from 200 to 700 μm. For each hole diameter, drops with two to four different volumes are tested, and we carry out five experiments for each volume. We can notice the remarkable repeatability for all the cases of the hole diameter and the drop volume.

As seen from Figs. 6 and 7, the experimental curves exhibit the following features. (i) For a fixed value of the hole diameter, the depletion time of the drop increases with its initial volume. For example, when $d = 200$ μm, t_0 increases from ∼140 ms for $\Omega_0 = 3.8$ μl to ∼1.22 s for $\Omega_0 = 25$ μl. However, for a fixed value of the drop volume, the depletion time of the drop decreases with the hole diameter. For example, when $\Omega_0 = 9.5$ μl, t_0 decreases from ∼6.6 s for $d = 100$ μm to ∼70 ms for $d = 700$ μm. (ii) For each case, oscillations are observed during the drainage of the drop, and the frequency increases with time while the amplitude decreases. Generally, the oscillations are more pronounced for larger initial drop volume (for a fixed hole diameter) or larger hole diameter (for a fixed drop volume). This phenomenon is remarkably different not only from the oscillation behaviors of sessile drops with fixed volumes [34–36], but also from the meniscus oscillations in capillary tubes around a fixed value of equilibrium height/depth [19,23,37]. (iii) Based on the five curves for each case with a fixed hole diameter and a fixed drop volume, Figs. 6 and 7 show that the repeatability of the experiment is extremely good, even though we could not quantitatively characterize the initial perturbation.

B. Theory

In this section, we put forward theoretical analyses to understand the drainage dynamics we have observed in the above. Here, we want to emphasize that, we first take $D(t)$ as the average value of the

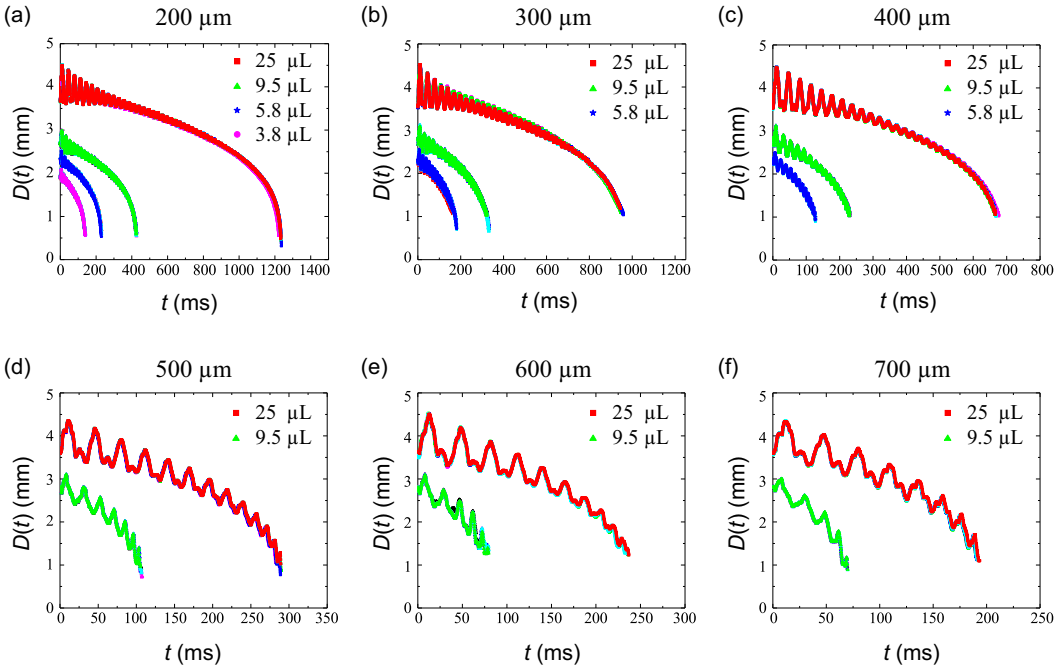

FIG. 7. Evolution of the drop diameter by employing Al plates with hole diameters ranging from 200 to 700 μm, as shown in panels (a)–(f), respectively. Drops with different volumes are tested, and there are five experiments carried out for each volume.

instantaneous diameter of the drop, and we will take the oscillation behaviors into consideration in the next section. Because of the surface tension and the curvature of the drop surface, the pressure difference (i.e., the Laplace pressure $\Delta P = P_{\text{in}} - P_0$) between the liquid in the drop P_{in} and the environment P_0 exists [16]. Since the surface of water in the container is flat, the pressure on the top of the bath is equal to the ambient pressure P_0. When the drop touches the hole, the Laplace pressure ΔP drives a flow, which accounts for the drainage of the drop and the appearance of the jet. For the sake of simplicity, we adopt the shape of the drop as spherical, and we obtain

$$\Delta P = \frac{2\sigma}{R(t)}, \tag{1}$$

where $R(t) = D(t)/2$ represents the average value of the instantaneous radius of the drop on its equatorial plane.

Assuming that the viscous dissipation could be neglected, for a certain moment t, we can describe the dynamics using the Bernoulli's principle at a given time t, i.e., $P_{\text{in}} = P_0 + [\rho U(t)^2)]/2$, in which ρ is the mass density of water and $U(t)$ is the instantaneous velocity of water through the hole. However, strictly speaking, the flow of our study is not perfectly inviscid. As a consequence, although the Al plates are very thin, $U(t)$ is not uniform around the hole. Therefore, we use a modified version of Bernoulli's principle to connect P_{in}, P_0, and $U(t)$,

$$P_{\text{in}} = P_0 + \tfrac{1}{2}\alpha\rho U(t)^2, \tag{2}$$

where α is an unknown factor to correct the relationship, and we assume α to be constant during the drainage with given values of the initial drop diameter and the hole diameter. Based on these

analyses, the dynamic equation could be built by balancing the capillary and inertia effects,

$$\frac{2\sigma}{R(t)} = \frac{1}{2}\alpha\rho U(t)^2. \tag{3}$$

Moreover, the conservation of volume flux during the drainage of the drop can be written as

$$-4\pi R^2(t)\frac{dR(t)}{dt} = AU(t), \tag{4}$$

where $A = \pi(d/2)^2$ is the cross-section of the hole. A combination of Eqs. (3) and (4) leads to

$$-\frac{dR(t)}{dt} = c_1 \cdot \frac{1}{R^{5/2}(t)}, \tag{5}$$

in which $c_1 = [\sigma A^2/(4\pi^2\alpha\rho)]^{1/2}$ is a coefficient. With respect to the boundary condition $R(t=0) = R_0$, a further integration of Eq. (5) leads to

$$R(t) = \left(R_0^{7/2} - \frac{7}{2}c_1 t\right)^{2/7} = \left(\frac{7}{2}c_1\right)^{2/7} \cdot (t_0 - t)^{2/7}, \tag{6}$$

where we have $t_0 = (2/7){R_0}^{7/2}/c_1$ from the boundary condition $R(t=t_0) = 0$. Moreover, based on the expression we have found for c_1, we further obtain

$$t_0 = \frac{4\pi}{7}\left(\frac{\rho}{\sigma}\right)^{1/2}\frac{\alpha^{1/2}R_0^{7/2}}{A} \approx 1.8\left(\frac{\rho}{\sigma}\right)^{1/2}\frac{\alpha^{1/2}R_0^{7/2}}{A}. \tag{7}$$

From a theoretical point of view, Eqs. (6) and (7) are closed-form solutions of the drainage of the drop, and α is the sole unknown factor (but may relate to R_0 and A). Since σ, A, ρ, and R_0 are known, and t_0 can be measured directly from the experiments, we could determine the values of α, as well as c_1. Moreover, based on an estimation of α, we could predict the depletion time t_0. However, in actual experiments, neither α nor t_0 could be precisely determined. The value of α would vary with time because of the time-dependent influence of the viscous dissipation and the velocity distribution around the hole. Moreover, when the diameter of the drop reaches the diameter of the hole, the solid-liquid-vapor three-phase contact line pins at the edge of the hole, such we cannot measure $R(t)$ and t_0 directly. For each curve in Figs. 6 and 7, we end the measurement of $D(t)$ when the drop is close to a hemisphere. Finally, we find α and t_0 by fitting the experiment data with Eq. (6). To exhibit the scaling nature of the problem, we reorganize Fig. 7 into Fig. 8 using the log-log plots. All the data follow the scaling $D(t) \sim (t_0 - t)^{2/7}$ very well, and the oscillations do not change this conclusion.

Here, we discuss further about the rationalization of our understandings in the above discussion, especially the modified version of Bernoulli's principle we have used. First, we define the Reynolds number as $\mathrm{Re} = \rho U d/\eta$, where $\eta \approx 0.001$ Pa·s is the dynamic viscosity of water. Strictly speaking, Re varies with time because of the nonconstant volume flux through the hole. Here, by calculating the characteristic velocity through $U \approx \Omega_0/(At_0)$, we give an estimation of the characteristic value of Re, where we approximate t_0 as the moment that the experimental data ends (see Figs. 6 and 7). In this way, and meanwhile considering the drop volume we use, we estimate that $\mathrm{Re} > 200$ when $d \in [500\,\mu\mathrm{m},\ 700\,\mu\mathrm{m}]$, $\mathrm{Re} > 100$ when $d \in [200\,\mu\mathrm{m},\ 400\,\mu\mathrm{m}]$, and $\mathrm{Re} \approx 20$ when $d = 100\,\mu\mathrm{m}$. So, we conclude that the viscous force does not play a significant role when the liquid flows through the hole. For a certain volume (i.e., $\Omega_0 = 9.5\,\mu\mathrm{l}$, see Fig. 9 in the next section and Table S1 in the Supplemental Material [33]), the values of α are obtained by fitting, and for most cases, the values of α are very close to 1.0, which suggests that the model we have constructed is acceptable.

C. Oscillation of the drop

We are interested in the oscillation behaviors because of their ubiquity during the drainage of the drop (see movies 1–4 in the Supplemental Material [33]). Here, we quantify the oscillation

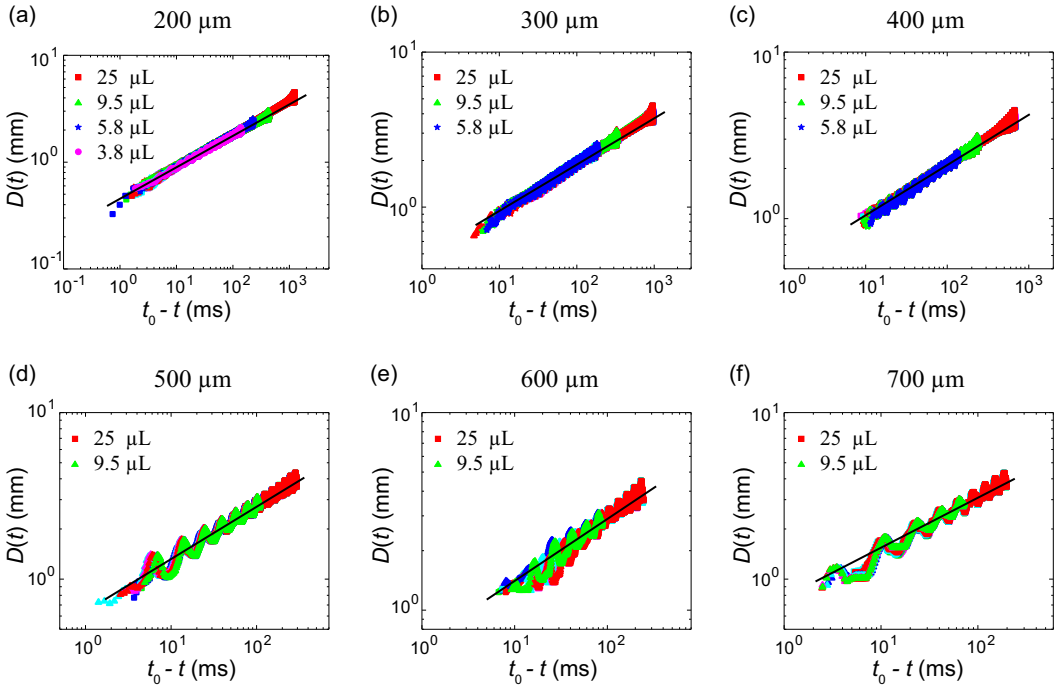

FIG. 8. Log-log plots showing the comparisons between the experimental data (dots) and $D(t) \sim (t_0 - t)^{2/7}$ (solid lines). The arrangement of the subgraphs corresponds to Fig. 7.

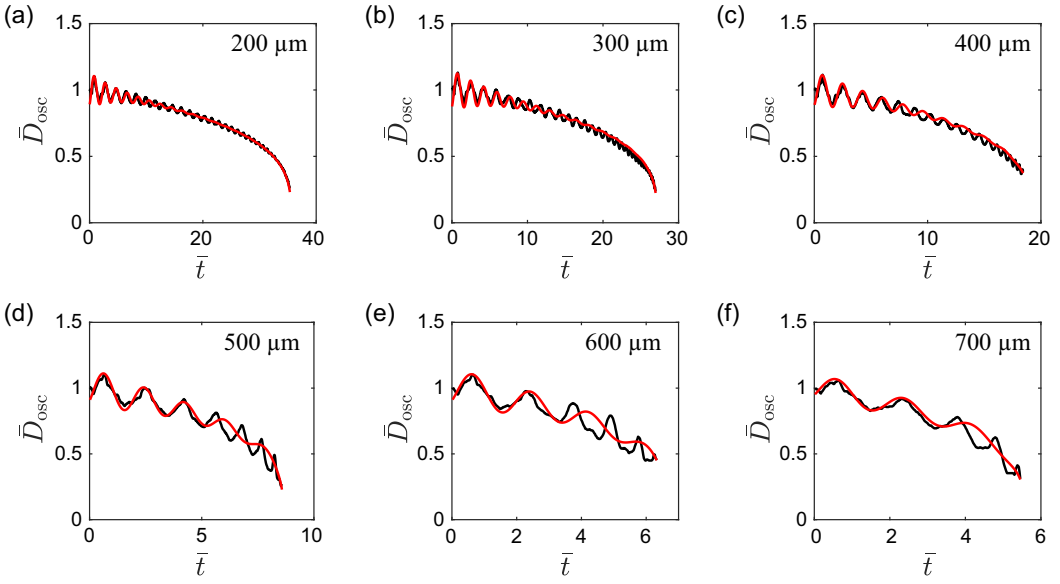

FIG. 9. Comparisons between the experimental data (in black) and the theoretical model (in red). The hole diameter ranges from 200 to 700 μm, as shown in panels (a)–(f), respectively. The volumes of the drops are fixed at 9.5 μl.

behavior by a combination of the mechanism of a damped harmonic oscillator and a scaling analysis. Such an attempt has been widely employed to understand the oscillation phenomena of liquids, such as coalescence of bubbles and drops [38–42], pending and sessile drops [36,43,44], liquids in confinements [24,45], etc.

For convenience, we use the theoretical models employed in previous works [36,38,39,42,45], but with necessary modifications considering the variable mass of the drop in our problem. The differential equation of a damped harmonic oscillator is as follows:

$$m\ddot{\Delta}(t) + b\dot{\Delta}(t) + k\Delta(t) = 0, \tag{8}$$

where $\Delta(t) = D_{\rm osc}(t) - D(t)$. We use $D_{\rm osc}(t)$ to denote the instantaneous diameter of the drop in its equatorial plane and to differentiate it from its average value $D(t)$ at a certain moment. m is the drop mass, b is the damping coefficient, and k is the spring constant. The magnitude of the relevant parameters could be identified by a scaling analysis, i.e., $m \sim \rho R^3$, $b \sim \eta R$, and $k \sim \sigma$. Here, we have to emphasize that the drop mass is changing with time, so our problem is quite different from the previous works in which certain values of the liquid mass were considered [38–45]. Face such a situation, we solve the problem along the following line of thought: we assume that $D_{\rm osc}(t)$ could be decoupled by a steady flow (i.e., $D(t)$ in the last section) and a damped harmonic oscillator $\Delta(t)$ with a certain volume. As a result, we write the approximate solution of Eq. (8) in dimensionless as

$$\bar{D}_{\rm osc}(t) = \bar{D}(t) + a_1 \exp\left(-a_2 \cdot {\rm Oh} \cdot \bar{t}\right) \cdot \sin\left(\frac{2\pi}{a_3} \cdot \bar{t} + \varphi\right), \tag{9}$$

where $\bar{D}_{\rm osc}(t) = D_{\rm osc}(t)/D_0$, $\bar{D}(t) = D(t)/D_0$, $\bar{t} = t/t^*$. t^* is the capillary time and defined as $t^* = (\rho\Omega_0/\sigma)^{1/2}$ [46]. The Ohnesorge number is defined as ${\rm Oh} = [\eta^2/(\rho\sigma R_0)]^{1/2}$ and its value is quite small (see Table S1 in the Supplemental Material [33]). a_1, a_2, a_3, and φ are coefficients. Strictly speaking, since the drop mass is time-dependent, the values of Oh and t^* might be also time-dependent, as well as the coefficients a_1, a_2, and a_3. To make the problem simpler, we use constant values of Oh and t^* as defined, and we also assume the values of a_1, a_2, and a_3 are constant in each case and we determine them by fitting the experimental data (see the Supplemental Material [33]).

To check the generality of our model, as shown in Fig. 9, we give comparisons between the experimental (black curves) and the theoretical results [red curves, Eq. (9)] with the hole diameters ranging from 200 to 700 μm. The initial volumes of all the drops are $\Omega_0 = 9.5$ μl. We can see that Eq. (9) reproduces the experimental results reasonably well in the first several periods, and it is not surprising that deviations happen at the later stage. To more closely capture the oscillation behaviors in the later stage, the time-dependent property of the parameters such as Oh, t^*, a_1, a_2, and a_3 has to be considered. The approximate models we have built for the oscillation analyses could be treated as a preliminary trying. More elaborate theories on the basis of the Navier-Stokes equation need to be developed in the future, and then the oscillation problem would be solved from the source.

Moreover, we also measure the value of the depletion time experimentally, denoting as $t_{0\_\rm exp}$. Then, we put $t_{0\_\rm exp}$ and t_0 (obtained via Eq. (7) based on the value of a found through a fitting from the experimental data, see the Supplemental Material [33]) into Fig. 10 to make a comparison. The black straight line represents the equality of the axes of the plot, and is used to guide the eye. We can see that the quantities obtained theoretically follow very well with the experimental measurements.

IV. LIQUID PUDDLES

In the previous experiments, the drop was small when compared with the capillary length and its shape was therefore spherical. We now focus on drops of large volume, i.e., puddles. However, the method presented before cannot be used in this case. On the one hand, when the volume of the drop is large enough, it will detach the needle because of the Rayleigh-Plateau instability [47]. On the other hand, when the falling drop touches the hole, drainage starts and we could not continue to statically add water into the drop to create a very large volume. To solve the problem, we herein

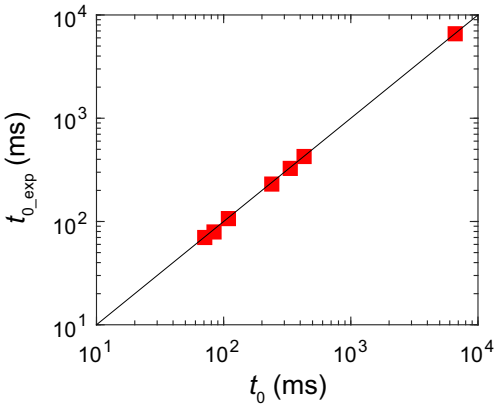

FIG. 10. Comparison between the depletion time of the theoretical results t_0 and the experimental measurements t_{0_exp}. The black line is used to guide the eye. Error bars are smaller than the symbol size.

employ a different way. First, we lift the Al plate to guarantee there is a gap between it and the bath of water. Then, we deposit sufficient water around the hole on the upper side of the Al plate. Since the hole is very small and both sides of the Al plate are superhydrophobic, there is no leakage of water from the hole. After that, we wait a while until the drop is steady. Then we carefully lower the position of the Al plate to let it touch the bath of water in the container. From this moment, drainage of the drop starts to happen. By employing this method, we could not only significantly increase the drop volume and create big puddles, but we could also largely suppress the initial perturbation and the oscillation of the liquid during the drainage (see movies 9 and 10 in the Supplemental Material [33]).

In Fig. 11, we show the new results obtained with large puddles, and compare them with the results of small drops. Six drops/puddles with initial diameters D_0 on their equatorial plane ranging from 2.66 to 17.72 mm are employed, and the hole diameter is kept at 200 μm. For the big puddle as shown in the second panel of Fig. 11(a), when drainage starts, the variation of its height is not obvious compared with its width. After some time (∼75 s), it gradually approaches a spherical shape like a drop with a small initial volume as shown in the first panel of Fig. 11(a). We give the evolution of the diameters of the drops and puddles in Figs. 11(b) and 11(c) linear and log-log plots, respectively. It is interesting to see that the drainage of the big puddle obeys a scaling relation $D(t) \sim (t_0 - t)^{1/2}$ in the early stage, and then follows $D(t) \sim (t_0 - t)^{2/7}$ when it becomes small enough. Moreover, during the whole drainage process, the oscillation behavior is significantly suppressed.

The new scaling relation $D(t) \sim (t_0 - t)^{1/2}$ could be obtained by the following arguments. For big puddles, its height is close to $2l_c$, where l_c is the capillary length defined by $l_c = (\sigma/\rho g)^{1/2}$ [16], denoting g the gravitational acceleration. For water at the ambient environment, $l_c \approx 2.73$ mm. Similar to the analyses in the last section, the pressure difference which drives the liquid could be written as

$$\Delta P = \frac{\sigma}{l_c}, \tag{10}$$

and then we build the dynamic equation

$$\frac{\sigma}{l_c} = \frac{1}{2}\alpha\rho U(t)^2. \tag{11}$$

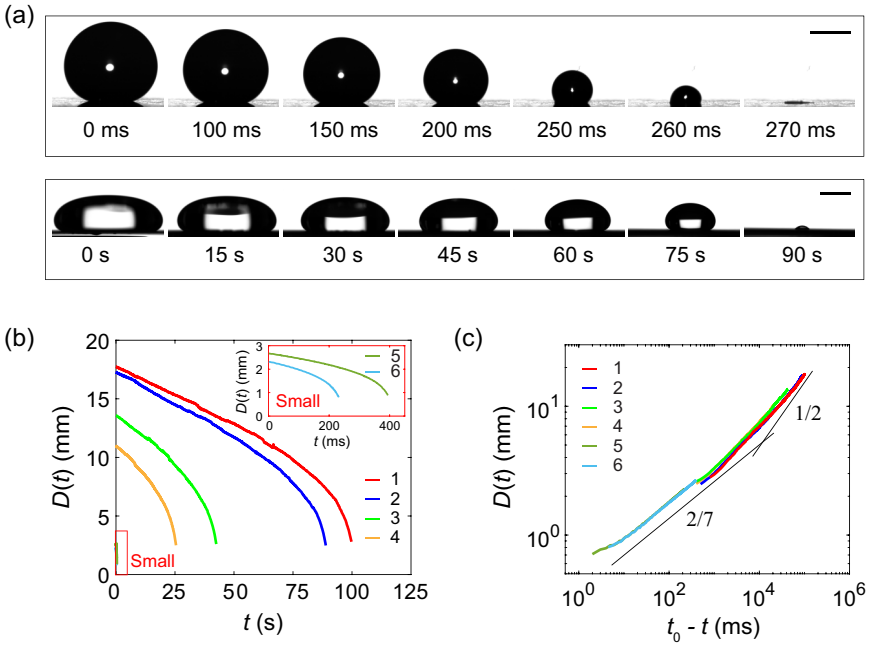

FIG. 11. Evolution of drops/puddles with different initial sizes. (a) Comparison of the drainage processes between a small drop and a big puddle. The scale bars represent 1 and 5 mm, respectively. Linear (b) and log-log (c) plots showing the relationships between $D(t)$ and t, and between $D(t)$ and $(t_0 - t)$, respectively. The inset in (b) is an enlargement for the small drops. The solid lines in (c) represent $D(t) \sim (t_0 - t)^{2/7}$ and $D(t) \sim (t_0 - t)^{1/2}$, respectively. Legend numbers 1–6 represent the initial diameter of the puddles/drops, i.e., $D_0 = 17.72$, 17.27, 13.57, 10.97, 2.66, 2.27 mm, respectively.

In this case, we have the following conservation of volume flux during the drainage of the puddle:

$$-4\pi l_c R(t)\frac{dR(t)}{dt} = AU(t). \tag{12}$$

Here, we emphasize that $R(t)$ is the instantaneous radius of the puddle on its equatorial plane. A combination of Eqs. (11) and (12) leads to

$$-\frac{dR(t)}{dt} = c_2 \cdot \frac{1}{R(t)}, \tag{13}$$

where $c_2 = [\sigma A^2/(8\pi^2 {l_c}^3 \alpha\rho)]^{1/2}$ is a factor. Regarding the boundary condition $R(t = 0) = R_0$, a further calculation of Eq. (13) leads to

$$R(t) = \left(R_0^2 - 2c_2 t\right)^{1/2} = (2c_2)^{1/2}(t_1 - t)^{1/2}, \tag{14}$$

where we define a factor $t_1 = {R_0}^2/(2c_2)$. However, Eq. (14) only represents the early time of the drainage process, c_2 (or α) are found out through fitting a part of the experimental data. Then, on the basis of c_2 and R_0, we could calculate t_1, and the physical meaning of t_1 is the moment that the $1/2$ scaling ends up.

As shown in Fig. 11(c), the experimental data of large puddles in the early time follow the $1/2$ scaling as Eq. (14) predicts. However, the $1/2$ scaling law in the log-log plot is not so remarkable when compared with the $2/7$ one. To extend the $1/2$ scaling regime to more decades, extremely large puddles are needed to prepare, which is challenging for the present experiment.

V. CONCLUDING REMARKS AND OUTLOOK

In summary, we have investigated the drainage and oscillation behaviors of drops driven by capillary flow through a hole. Due to the size-dependent Laplace pressure resulting from the variable mass of the drop, scaling relations of the drainage of the drop diameter with time have been identified. For small drops, we reveal that $D(t) \sim t^{2/7}$ is obeyed globally during the whole drainage process, whereas for big puddles, we reveal that the drainage obeys $D(t) \sim t^{1/2}$ and $D(t) \sim t^{2/7}$ in the early and latter stages, respectively. Experimental and theoretical results are in good agreement. Moreover, based on scaling analyses, we have modeled the drop as a damped harmonic oscillator under the initial perturbation and with variable mass, and the theoretical results finely follow the experimental data. We expect our results will find practical applications, for instance, in the field of liquid transport, oil extraction, interstitial flow, oil/water separation and so on. Furthermore, we hope our work will deepen our knowledge about the damped oscillator with variable mass driven by capillary forces. It would be interesting to extend our results to the case of viscous or non-Newtonian liquids. Further studies should be devoted to examining the complex dynamics and instability of the jet inside the bath of water.

ACKNOWLEDGMENTS

C.L. acknowledges the financial support from the National Natural Science Foundation of China (Grants No. 11632009, No. 11872227, No. 11921002), the financial support from Tsinghua University (Grant No. 100301011), and the support from the Young Overseas High-level Talents Introduction Plan. S.S. and C.L. thanks Maosheng Chai and Pengfei Hao for AFM and micro-PIV testing supports, respectively. P.J. thanks the support from Harbin Institute of Technology in Shenzhen (Grant No. HA45001103). The authors are grateful to Prof. Howard Stone and Prof. Dominic Vella for the stimulating discussions. We are grateful to the anonymous reviewers whose suggestions have helped to significantly improve the paper.

[1] M. Prakash, D. Quéré, and J. W. Bush, Surface tension transport of prey by feeding shorebirds: The capillary ratchet, Science **320**, 931 (2008).
[2] A. Rico-Guevara and M. A. Rubega, The hummingbird tongue is a fluid trap, not a capillary tube, Proc. Natl. Acad. Sci. USA **108**, 9356 (2011).
[3] K. Piroird, C. Clanet, and D. Quéré, Detergency in a tube, Soft Matter **7**, 7498 (2011).
[4] K. Piroird, C. Clanet, and D. Quéré, Capillary extraction, Langmuir **27**, 9396 (2011).
[5] K. P. Hapgood, J. D. Litster, S. R. Biggs, and T. Howes, Drop penetration into porous powder beds, J. Colloid Interface Sci. **253**, 353 (2002).
[6] B. Lavi, A. Marmur, and J. Bachmann, Porous media characterization by the two-liquid method: Effect of dynamic contact angle and inertia, Langmuir **24**, 1918 (2008).
[7] J. Bachmann, S. Woche, M. O. Goebel, M. Kirkham, and R. Horton, Extended methodology for determining wetting properties of porous media, Water Resour. Res. **39**, 1353 (2003).
[8] M. Lazghab, K. Saleh, I. Pezron, P. Guigon, and L. Komunjer, Wettability assessment of finely divided solids, Powder Technol. **157**, 79 (2005).
[9] D. J. Durian, D. Weitz, and D. Pine, Scaling behavior in shaving cream, Phys. Rev. A **44**, R7902 (1991).
[10] Z.-G. Cui, B. P. Binks, and J. H. Clint, Determination of contact angles on microporous particles using the thin-layer wicking technique, Langmuir **21**, 8319 (2005).
[11] T. D. Wheeler and A. D. Stroock, The transpiration of water at negative pressures in a synthetic tree, Nature **455**, 208 (2008).
[12] J. Comtet, K. H. Jensen, R. Turgeon, A. D. Stroock, and A. Hosoi, Passive phloem loading and long-distance transport in a synthetic tree-on-a-chip, Nat. Plants **3**, 17032 (2017).

[13] E. Bazzo and M. Nogoseke, Capillary pumping systems for solar heating application, Appl. Therm. Eng. **23**, 1153 (2003).
[14] G. Walker and D. J. Beebe, A passive pumping method for microfluidic devices, Lab Chip **2**, 131 (2002).
[15] L. Gervais and E. Delamarche, Toward one-step point-of-care immunodiagnostics using capillary-driven microfluidics and PDMS substrates, Lab Chip **9**, 3330 (2009).
[16] P.-G. De Gennes, F. Brochard-Wyart, and D. Quéré, *Capillarity and Wetting Phenomena: Drops, Bubbles, Pearls, Waves* (Springer Science & Business Media, Berlin, 2003).
[17] R. Lucas, Ueber das zeitgesetz des kapillaren aufstiegs von flüssigkeiten, Kolloid-Z. **23**, 15 (1918).
[18] E. W. Washburn, The dynamics of capillary flow, Phys. Rev. **17**, 273 (1921).
[19] D. Quéré, Inertial capillarity, Europhys. Lett. **39**, 533 (1997).
[20] N. Fries and M. Dreyer, The transition from inertial to viscous flow in capillary rise, J. Colloid Interface Sci. **327**, 125 (2008).
[21] N. Fries and M. Dreyer, An analytic solution of capillary rise restrained by gravity, J. Colloid Interface Sci. **320**, 259 (2008).
[22] A. Hamraoui, K. Thuresson, T. Nylander, and V. Yaminsky, Can a dynamic contact angle be understood in terms of a friction coefficient?, J. Colloid Interface Sci. **226**, 199 (2000).
[23] J. Delannoy, H. de Maleprade, C. Clanet, and D. Quéré, Capillary descent, Soft Matter **14**, 5364 (2018).
[24] H. Lim, A. Tripathi, and J. Lee, Dynamics of a capillary invasion in a closed-end capillary, Langmuir **30**, 9390 (2014).
[25] T. S. Ramakrishnan, P. Wu, H. Zhang, and D. T. Wasan, Dynamics in closed and open capillaries, J. Fluid Mech. **872**, 5 (2019).
[26] D. Schebarchov and S. Hendy, Dynamics of capillary absorption of droplets by carbon nanotubes, Phys. Rev. E **78**, 046309 (2008).
[27] S. Costa, E. Borowiak-Palen, A. Bachmatiuk, M. Rümmeli, T. Gemming, and R. Kaleńczuk, Filling of carbon nanotubes for bio-applications, Phys. Status Solidi A **244**, 4315 (2007).
[28] I. Mönch, A. Leonhardt, A. Meye, S. Hampel, R. Kozhuharova-Koseva, D. Elefant, M. Wirth, and B. Büchner, Synthesis and characteristics of Fe-filled multi-walled carbon nanotubes for biomedical application, in *Journal of Physics: Conference Series* (IOP Publishing, Bristol, UK, 2007), p. 820.
[29] M. Cao, K. Li, Z. Dong, C. Yu, S. Yang, C. Song, K. Liu, and L. Jiang, Superhydrophobic "pump": Continuous and spontaneous antigravity water delivery, Adv. Funct. Mater. **25**, 4114 (2015).
[30] S. Huang, J. Song, Y. Lu, C. Lv, H. Zheng, X. Liu, Z. Jin, D. Zhao, C. J. Carmalt, and I. P. Parkin, Power-free water pump based on a superhydrophobic surface: Generation of a mushroomlike jet and antigravity long-distance transport, J. Mater. Chem. A **4**, 13771 (2016).
[31] J. Song, F. Guan, W. Pan, Z. Liu, J. Sun, S. Ling, X. Deng, and Y. Sun, Droplet-based self-propelled miniboat, Adv. Funct. Mater. **30**, 1910778 (2020).
[32] R. Wen, S. Xu, D. Zhao, L. Yang, X. Ma, W. Liu, Y.-C. Lee, and R. Yang, Sustaining enhanced condensation on hierarchical mesh-covered surfaces, Natl. Sci. Rev. **5**, 878 (2018).
[33] See Supplemental Material at http://link.aps.org/supplemental/10.1103/PhysRevFluids.5.104002 for detailed descriptions of the analyses of the oscillation dynamics and the movies.
[34] J. B. Bostwick and P. H. Steen, Capillary oscillations of a constrained liquid drop, Phys. Fluids **21**, 233 (2009).
[35] P. S. Brown, A. Berson, E. L. Talbot, T. J. Wood, W. C. Schofield, C. D. Bain, and J. P. Badyal, Impact of picoliter droplets on superhydrophobic surfaces with ultralow spreading ratios, Langmuir **27**, 13897 (2011).
[36] R. M. Manglik, M. A. Jog, S. K. Gande, and V. Ravi, Damped harmonic system modeling of post-impact drop-spread dynamics on a hydrophobic surface, Phys. Fluids **25**, 082112 (2013).
[37] D. Quéré, É. Raphaël, and J.-Y. Ollitrault, Rebounds in a capillary tube, Langmuir **15**, 3679 (1999).
[38] R. L. Stover, C. W. Tobias, and M. M. Denn, Bubble coalescence dynamics, AlChE J. **43**, 2385 (1997).
[39] V. Chireux, D. Fabre, F. Risso, and P. Tordjeman, Oscillations of a liquid bridge resulting from the coalescence of two droplets, Phys. Fluids **27**, 062103 (2015).
[40] J. Zheng, H. Shi, G. Chen, Y. Huang, H. Wei, S. Wang, and W. Wen, Relaxation of liquid bridge after droplets coalescence, Aip Adv. **6**, 115115 (2016).

[41] Á. M. Soto, T. Maddalena, A. Fraters, D. Van Der Meer, and D. Lohse, Coalescence of diffusively growing gas bubbles, J. Fluid Mech. **846**, 143 (2018).
[42] R. Chen, J. Zeng, and H. Yu, Mechanism of damped oscillation in microbubble coalescence, Comput. Fluids **183**, 38 (2019).
[43] Y.-S. Shin and H.-C. Lim, Shape oscillation and detachment conditions for a droplet on a vibrating flat surface, Eur. Phys. J. E **37**, 74 (2014).
[44] R. H. Temperton, M. I. Smith, and J. S. Sharp, Mechanical vibrations of pendant liquid droplets, Eur. Phys. J. E **38**, 79 (2015).
[45] C. Lv, S. N. Varanakkottu, and S. Hardt, Liquid plug formation from heated binary mixtures in capillary tubes, J. Fluid Mech. **889**, A15 (2020).
[46] D. Richard, C. Clanet, and D. Quéré, Contact time of a bouncing drop, Nature **417**, 811 (2002).
[47] C. Clanet and J. C. Lasheras, Transition from dripping to jetting, J. Fluid Mech. **383**, 307 (1999).